ELSEVIER

Contents lists available at ScienceDirect

Computational Materials Science

journal homepage: www.elsevier.com/locate/commatsci



Full Length Article



Effects of misfit dislocations and dislocation mobility on thermal boundary resistance of PbTe/PbSe interfaces

Nicholas Taormina^a, Yang Li^a, Simon Phillpot^b, Youping Chen^{a,*}

- a Department of Mechanical and Aerospace Engineering, University of Florida, Gainesville, FL 32611, USA
- b Department of Materials Science and Engineering, University of Florida, Gainesville, FL, 32611, USA

ABSTRACT

We present a molecular dynamics study of the thermal transport properties of PbTe/PbSe (111) and PbTe/PbSe (100) interfaces at room temperature. The PbTe/PbSe heterostructures are obtained through simulations of the kinetic processes of direct bonding of PbTe and PbSe crystals. The atomic-scale dislocation core structures and the misfit dislocation networks in the heterostructures obtained in the simulations are found to closely match experimental data. Two types of heat transfer experiments are then simulated: a heat-sink heat-source experiment and an ultrashort heat pulse experiment. Thermal boundary resistance is calculated for three distinct interface types: coherent, semi-coherent, and semi-coherent with pinned dislocations. Both types of simulations consistently capture the significant role of the misfit dislocations on thermal resistance. The effect of the mobility of dislocations on thermal resistance is demonstrated for the first time through comparing the thermal boundary resistance of interfaces containing pinned dislocations and with those containing unpinned dislocations. In addition, the thermal boundary resistance is found to strongly depend on the length of the specimen and the area of the interface.

1. Introduction

Thermoelectric materials have garnered significant interest for their potential to convert heat into electricity [1,2]. The most effective thermoelectrics are materials with multiscale microstructures, in which interfaces link structural elements at different scales or between different materials or phases. One material that exemplifies a high thermoelectric figure of merit are the PbTe-based material systems, such as those that contain PbTe/PbSe interfaces, which stands out due to its comparably low thermal conductivity. This low thermal conductivity is achieved through two pathways: low conductivity of the PbTe and PbSe single crystals and pronounced thermal resistance at the interface between them. While the low thermal conductivity in bulk PbTe single crystals are believed to be caused by strong scattering of longitudinal acoustic phonons by optical phonons [3,4], the specific mechanisms through which the interfaces influence thermal conductivity, however, are incompletely explored. In particular, experimental observations using high-resolution transmission electron microscopy have observed the formation of misfit dislocation structures along the PbTe/PbSe heterointerface as a result of the incongruent lattice constants [5]. A quantitative understanding of the role of the misfit dislocations on thermal resistance remains limited.

Dislocations are crystallographic defects that play a vital role in a material's mechanical, thermal, and electronic properties. At lattice-

mismatched interfaces, misfit dislocations are observed and cannot be removed as they are an equilibrium defect, a product of the differences in lattice constants or crystal structure between the two materials. Because they are permanent, misfit dislocations are extremely important in materials or structures that contain different materials or phases, such as semiconductor heterostructures or thermoelectric materials interfaces.

These misfit dislocations scatter phonons, the major heat carriers of semiconductors or thermoelectric materials, thereby contributing to the interfacial thermal resistance, and consequently reducing the thermal conductivity of the materials or structures [6,7]. Despite the potentially important role they may play, misfit dislocations are often ignored in interfacial phonon transport studies. To date, the majority of existing computational studies of interfacial phonon transport assumed coherent interfaces or considered the interfacial roughness by changing the mass of atoms in the interfaces [8,9] or used interfacial species mixing [10,11] or diffusion [12]. These studies showed that the thermal conductivity of heterogeneous materials systems, such as Si/Ge superlattices, depends strongly on the structure of the interfaces. However, existing computational studies have not reproduced the experimentallymeasured thermal conductivity of semiconductor heterostructures such as the Si/Ge superlattices [13] or the GaN/AlN multilayers or heterointerfaces [14]. It was suggested by Lee and Cahill that interface misfit dislocations might be responsible for the low thermal conductivity of Si/

E-mail address: ypchen2@ufl.edu (Y. Chen).

 $^{^{\}ast}$ Corresponding author.

Ge superlattices measured in their experiments [13].

There are some recent studies on the role of misfit dislocations on thermal boundary resistance. Sun et al. simulated the direct bonding of GaN and AlN crystals using molecular dynamics simulations with three different interatomic potentials; each produced similar misfit dislocation network and dislocation core structures [15]. The misfit dislocations at the GAN/AlN interface were found to reduce the thermal boundary condutance by 47.1 %, 21.9 %, and 40.1 % using the different interatomic potentials [15]. Li et al. simulated the direct bonding of PbTe and PbSe (001) crystals [16], as well as the molecular beam epitaxy of PbTe /PbSe (001) and PbSe/PbTe (111) systems, and obtained the structure and density of misfit dislocations at the PbTe/PbSe interfaces [17], using the concurrent atomistic-continuum method [18–20]. Later they simulated phonon transport in their computationally obtained PbTe/PbSe (001) heterostructures and captured the resonant interaction between phonons and dislocations [21]. Their simulations illustrated the static and dynamic mechanisms and demonstrated the significant role of the dynamic interaction between phonons and misfit dislocation networks on energy transmission [21]. However, this study only investigated the PbTe/PbSe (001) heterostructures and did not directly measure the thermal boundary resistance

This study aims to provide a quantitative understanding on the role of misfit dislocations on interfacial thermal transport across the (111) and (100) PbTe/PbSe heterointerfaces. To quantify the role of misfit dislocations, three types of interfaces: coherent, semi-coherent, and semi-coherent with pinned dislocations, are simulated, with different interfacial areas and specimen lengths. The PbTe/PbSe system is selected for this study because it is a prominent thermoelectric material system, and also because the interatomic potentials for this material system are well-developed and have been shown to produce accurate results for dislocation structures and dispersion relations of acoustic phonons [16].

The paper is organized as follows. Following this introduction, in Section II, we first describe the computer models, the simulation setup, and parameters; we then present simulation results of the direct bonding processes of PbTe and PbSe crystals and the resulting misfit dislocation networks and dislocation core structure for each system. In Section III, we present simulation and calculation results of the thermal boundary resistance (TBR) of the various heterostructures obtained in the bonding simulations, as well as phonon wave packet simulation results of these heterostructures to provide quantitative information on energy transmission across the different interfaces as a function of phonon wavevector. This paper is concluded with a brief summary and discussion in Section IV.

2. Methodology

The Large-scale Atomic/Molecular Massively Parallel Simulator (LAMMPS) is employed for all the molecular dynamics (MD) simulations of the PbTe/PbSe systems in this work. All simulations in this study use the Buckingham-Coulombic interatomic potential based on the transferable force field for CdS-CdSe-PbS-PbSe solid systems [22]. This potential incorporates both the long-range Coulombic interaction and the short-range Buckingham interaction accounting for both the Pauli exclusion principle and van der Waals forces. The potential was further developed to include PbTe and has been demonstrated to be able to reproduce the dislocation structures in PbTe/PbSe systems [16,17,21], in good agreement with experimental measurements and observations [23,24], as well as the phonon dispersion relations for acoustic phonons in both PbTe and PbSe systems in good agreement with DFT calculations [21,22].

2.1. Direct wafer bonding

Direct wafer bonding is a manufacturing process to bond two solids

with sufficiently flat surfaces. It is widely used in the fabrication of electronic and optoelectronic devices. To obtain the defect structures at the PbTe/PbSe interfaces, the kinetic processes of direct wafer bonding are simulated in this work. This process consists of three steps. First, the structure for each individual crystal is created and relaxed to obtain the equilibrated single crystal structure. Second, an equilibrated single crystal is placed on top of another equilibrated single crystal at 300 K under significant pressure (150 bar) to create a bonded surface. Finally, the newly created heterostructure is annealed at 1000 K to fully relax the bonded heterostructure.

For the PbTe/PbSe system at 300 K using the Buckingham-Coulombic potential, the lattice mismatch is 5.1 %. Therefore, the smallest interface size for a minimum energy density model is 19 PbTe unit cells paired with 20 PbSe unit cells. A model of this size contains one Peierls-Nabarro dislocation network. To achieve an interface with 2x2 dislocation networks, the number of unit cells for each material is simply doubled in each in-plane direction. Based on this procedure, computer models of PbTe/PbSe (111) and PbTe/PbSe (100) systems with various interface areas and specimen lengths are constructed, respectively, including three different interfaces areas that consist of 38 by 38, 76 by 76, and 114 by 114 PbTe unit cells, respectively, and two different specimen lengths, 170 nm and 340 nm, for each computer model, respectively. Table 1 details the interface size of all the models that are used in this study.

For comparison, we also directly build computer models that contain coherent PbTe/PbSe interfaces. As a result of the inherent lattice mismatch in the PbTe/PbSe system, the coherent interface model must be limited in size to avoid the formation of misfit dislocations. It should be noted that such structures do not exist in real material systems. Nevertheless, they can be used to quantify the role of misfit dislocations. To facilitate a meaningful comparison, identical interfacial sizes of 6-unit cells by 6-unit cells are constructed for both the (100) and (111) coherent models. Fig. 1 presents the atomic structures of the coherent interfaces. It is noticed that the interfaces create a structural discontinuity in both systems. However, the (111) interface is less chemically discontinuous than the (100) interface, as the PbTe layer and PbSe layer in the former share one Pb layer, as shown in Fig. 1B.

For the semi-coherent interfaces, we simulate the direct bonding processes to obtain misfit dislocation networks at the heterointerface. The structures obtained through this technique are found to agree well with experimental observations. In Fig. 2, we present the dislocation core structures obtained in the direct bonding simulations, where the core atoms are indicated by the black box. All the misfit dislocations are edge dislocations with the Burgers vectors along $\langle 1\,1\,0\rangle$, with the slip planes being $\{1\,0\,0\}$ and $\{1\,1\,1\}$ for the two different systems, respectively. Note that these two interfaces have the same lattice mismatch and the same magnitude of Burgers's vector and hence the same misfit dislocation density at the interface. They differ in slip plane and dislocation core structure, as a dislocation in the $(1\,1\,1)$ interface has a $\{1\,1\,1\}$ slip plane, while the $(1\,0\,0)$ interface has a $\{1\,1\,0\}$ slip plane.

The Dislocation Extraction Algorithm (DXA) embedded in the OVITO visualizer software is employed to analyze the dislocation network formed in the simulation [25,26]. The (111) interface exhibits a dislocation network with units of hexagonal shape, while the (100) interface

Table 1The Interfacial Size of Each Model.

Crystal Orientation	Interface Size (nm by nm)					
	Coherent Interfaces	Semi- coherent 38 by 38 PbTe Unit Cells	Semi- coherent 76 by 76 PbTe Unit Cells	Semi-coherent 114 by 114 PbTe Unit Cells		
(111)	2.6 by 2.3	17.2 by 14.9	34.4 by 29.8	51.6 by 44.7		
(100)	3.8 by 3.8	24.5 by 24.5	49.0 by 49.0	73.6 by 73.6		

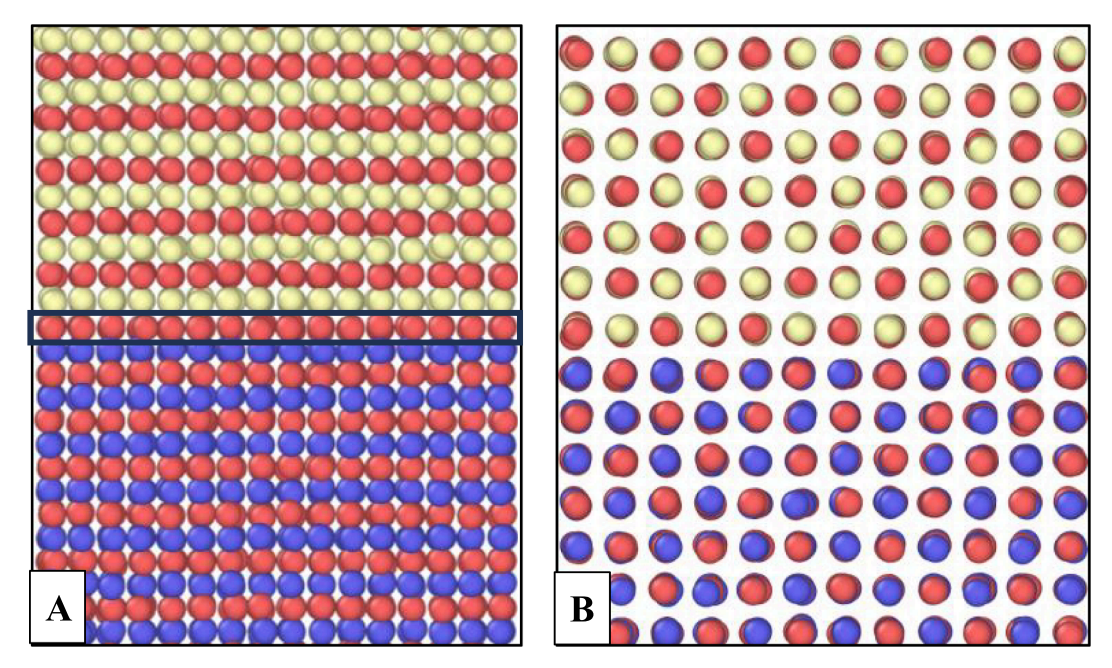


Fig. 1. A cross-sectional view of the (1 1 1) coherent interface (A) and (100) coherent interface (B) that contains 6 by 6 PbTe and PbSe unit cells. The red atoms represent lead, the yellow atoms represent tellurium, and the blue atoms represent selenium. (For interpretation of the references to colour in this figure legend, the reader is referred to the web version of this article.)

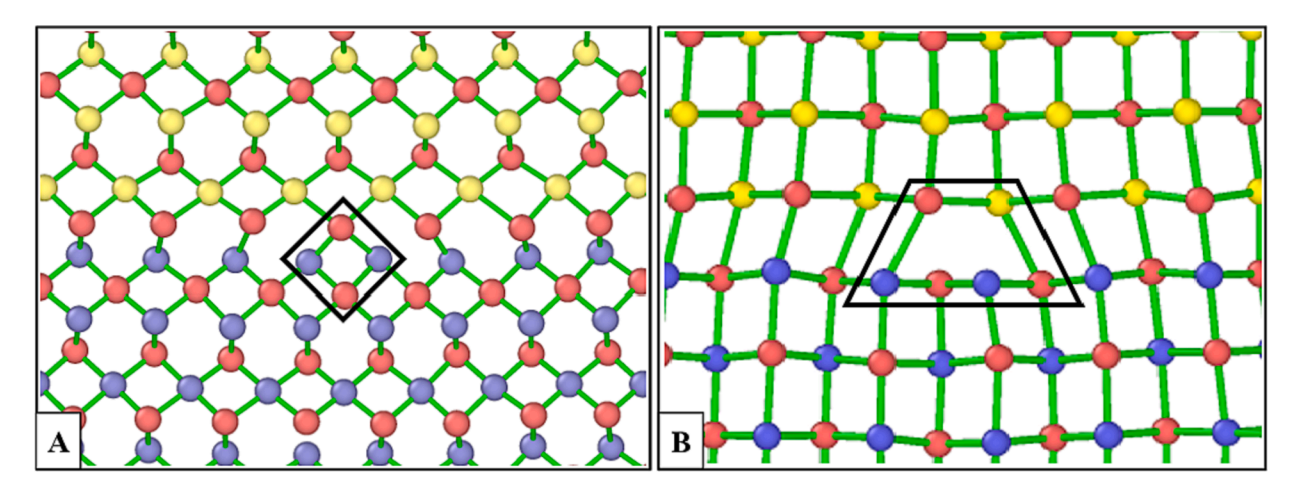


Fig. 2. Dislocation core structure displayed in the black box, for (A) (111) and (B) (100) interfaces. The red atoms represent lead, the yellow atoms represent tellurium, and the blue atoms represent selenium. (For interpretation of the references to colour in this figure legend, the reader is referred to the web version of this article.)

displays units with a diamond-shape, as shown in Fig. 3. A comparison with experimental observations is presented in Fig. 3(B), highlighting the close resemblance between the simulated and real-world interfacial structures.

2.2. Pinning dislocations

To quantify the role of dislocation mobility, point defects are introduced into the bonded heterostructures to pin the movement of the misfit dislocations. This is accomplished by removing atoms along segments of the misfit dislocation network to simulate the effects of gamma radiation, which is an experimental technique to immobilize dislocations [27,28]. Gamma radiation pins down mobile dislocations without removing them, therefore allowing the effects of dislocation mobility to be studied. For this purpose, two computer models of length 340 nm with pinned dislocations are created with the interface containing 38 by 38-unit cells, and 114 by 114-unit cells, respectively. Specifically, 12

atoms are excised from each dislocation segment within each model. Subsequent phonon wave propagation simulations are conducted to evaluate the effectiveness of this pinning technique [21]. The amplitude of dislocation network vibrations is diminished by over 25 % in the pinned models relative to the unpinned models, indicating that the pinning has reduced some, not all of, the dislocation mobility. Since the vacancies introduced via this method can also influence the thermal boundary resistance, simulations are conducted on a coherent interface model featuring vacancies to quantify the effect of the vacancies, thereby allowing the impact of dislocation mobility to be more accurately measured in later simulations.

2.3. Direct heat source-sink method

Once all the models have been created and the interfacial structures are verified, the nonequilibrium molecular dynamics method that models the direct heat-source-heat sink experimental technique is used

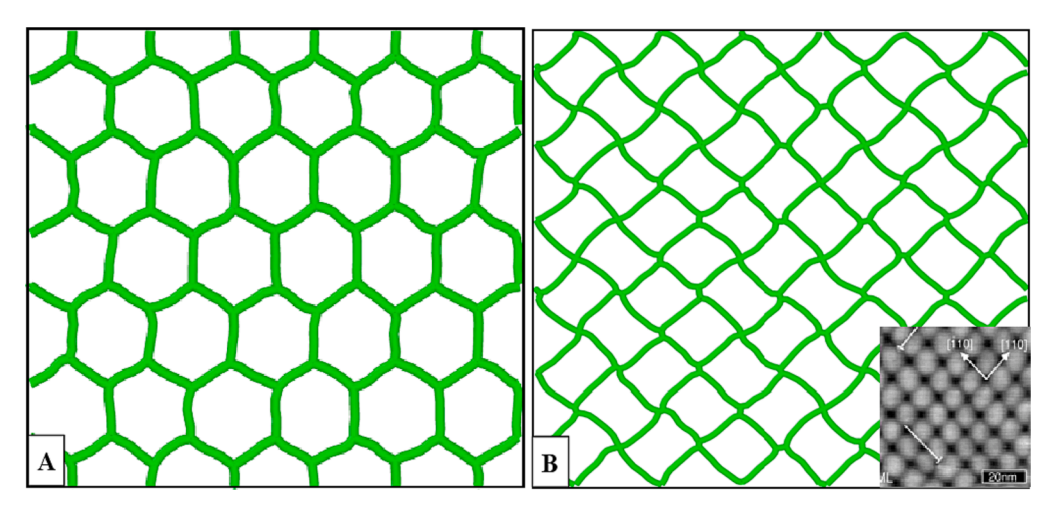


Fig. 3. Misfit dislocation networks for the PbTe/PbSe (A) (111) and (B) (100) interfaces. The inset in (B) is a scanning tunneling microscopy image of the PbTe/PbSe (100) semi-coherent interface [5]. The (111) interface produces clear hexagonal networks, while the networks in the (100) interface are diamond shaped. The dislocation lines in the (100) network become straight at higher temperatures.

to simulate the steady state of the system under a constant heat flux at an average temperature of 300 K [29]. In this method, the atoms in the model are grouped according to their position along the length of the specimen with the intent to denote an observable path for heat flow through the model. A simplified 2-D view of the direct method simulation setup is presented in Fig. 4.

A heat source and a heat sink region of equal size are designated at opposing ends of the model. The heat flux of the source and sink are set to equal and opposite values to ensure conservation of energy and the eventual generation of a steady-state temperature profile. Each simulation is allowed to run until the system reaches a steady state, i.e., the time-averaged temperature profile no longer changes with time. An example of such a temperature profile is presented in Fig. 5. The sharp drop at the interface, i.e., the midpoint of the X-axis, represents the temperature drop due to the thermal boundary resistance. This temperature drop, ΔT , along with the heat flux, J, and the interfacial area A used in the simulation, are used to calculate the thermal boundary resistance, i.e.,

$$R = \frac{\Delta T}{J}$$

where

$$J = \frac{\Delta \varepsilon}{A \Delta t} \tag{1}$$

Both the heat flux and interfacial area are input properties of the model, while the change in temperature is a result of the simulation. The exact temperature is determined by fitting a line to the temperature profile points on either side of the interface and comparing their predicted values at the interfacial midpoint. This method of calculating thermal boundary resistance has been extensively tested and shown to

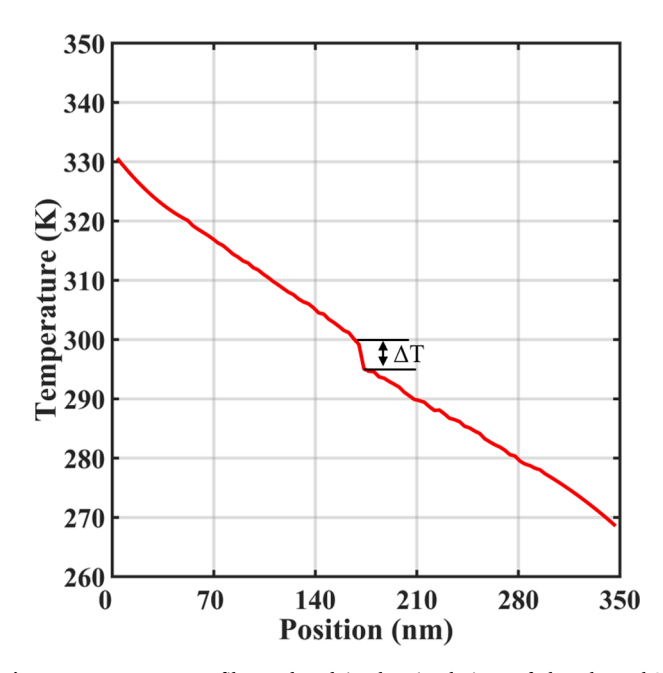


Fig. 5. Temperature profile produced in the simulations of the PbTe/PbSe (100) model with an interface size of 114 by 114-unit cells and a length of 340 nm. The sharp drop at the center is a result of phonon scattering by the interface.

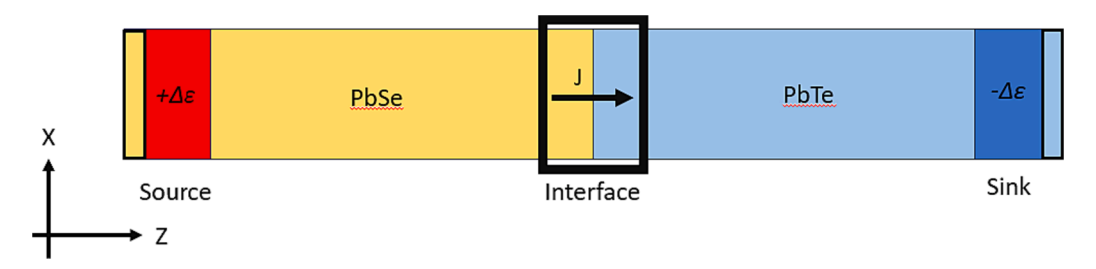


Fig. 4. An overview of the simulation setup for the direct heat-source-heat-sink method simulations, in which J represents the applied heat flux and $\Delta \epsilon$ is the added energy to the heat source region and subtracted from the heat sink region per time step.

produce results similar to those observed in real applications [30].

2.4. Phonon wave packet propagation

The heat-source-heat-sink method-based simulations directly measure thermal conductance or thermal resistance of a system or of an interface. To seek more information of the phonon transport across the interfaces, simulation of the propagations of phonon wave packets, with wavelength ranging from the minimum wave length 2a to the maximum wavelength, 2L, where a is the equilibrium separation between atoms and L is the maximum length of the specimen [31–33], are conducted to quantitatively assess the interaction between phonons and misfit dislocations. Both (111) and (100) models with 38 by 38 unit cells are used in these simulations. By comparing the results of the two models, further insights can be obtained into the phonon-dislocation interactions at the interface.

The computer models are cooled to a temperature near 0 K to minimize anharmonic phonon–phonon scattering and focus on phonon-interface scattering. While achieving relaxation to absolute zero energy is impossible, the models are allowed to reach an acceptable minimum temperature of less than 10^{-7} K with the maximum atomic force to be

less than 10⁻⁸ eV/Å. The resulting background energy in the relaxed model is recorded to facilitate subsequent data calculations. Following the relaxation, a phonon wave packet is introduced in the PbSe side of the heterostructure and propagates along the Z direction. As the phonon wave packet passes across the interface, a portion of the packet is reflected back by the interface. A series of such simulations are conducted to measure the energy transmission coefficient of the longitudinal acoustic (LA) and transverse acoustic (TA) phonons. All these simulations are performed at a very low temperature to avoid anharmonic phonon–phonon scattering, thereby enabling the quantification of the role of misfit dislocations and interactions.

To calculate the energy transmission coefficients, the total energy of the specimen before the phonon passes through the interface is compared to the total energy afterward. The energy specific to the phonon is obtained by subtracting the energy present in the model prior to the introduction of the phonon. This technique reduces the influence of background phonons in the model, allowing the phonon wave packet alone to be quantified.

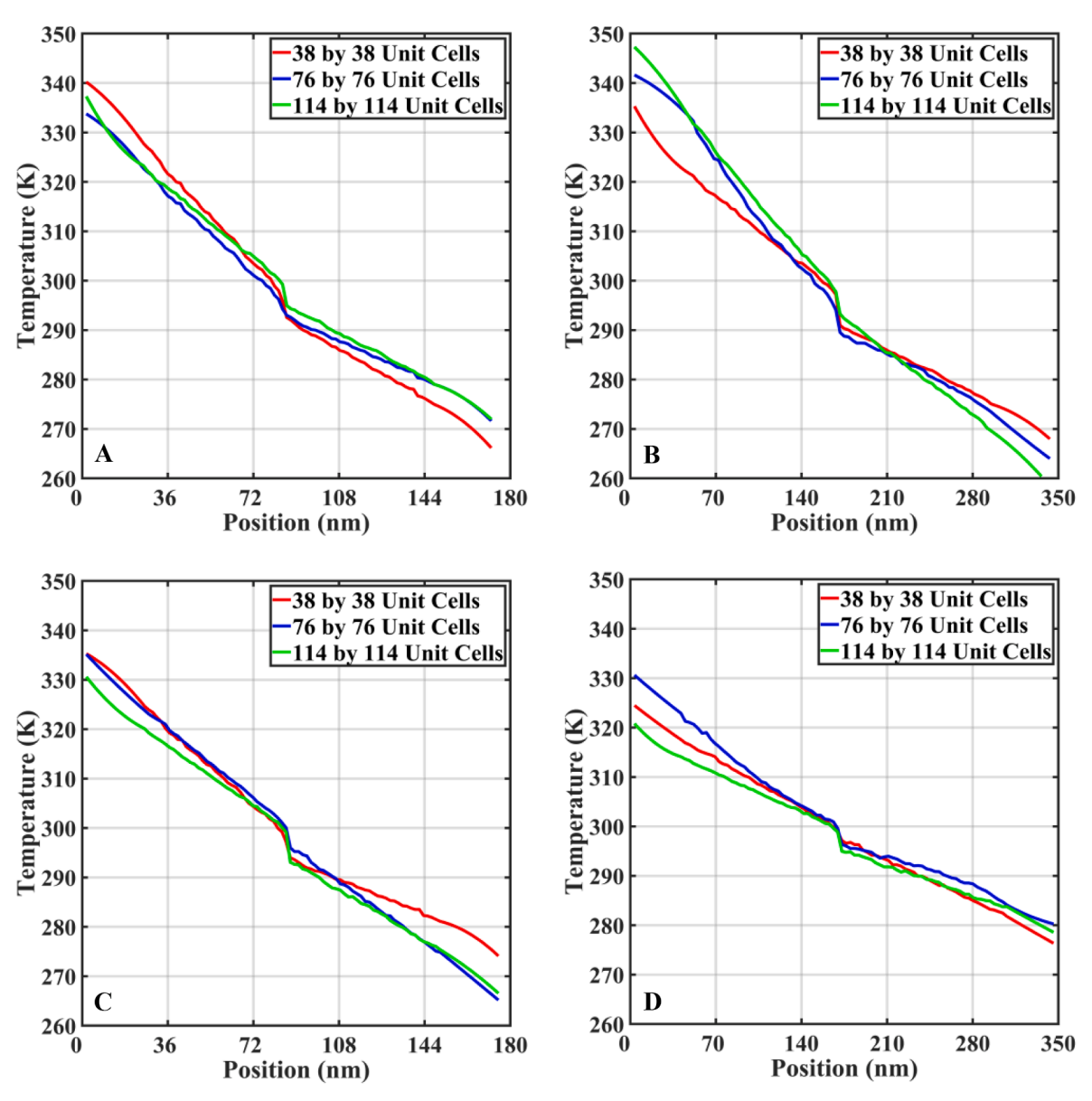


Fig. 6. The temperature profiles for (A) (111) 170 nm model, (B) (111) 340 nm model, (C) (100) 170 nm model, and (D) (100) 340 nm model.

3. Thermal transport simulation results

3.1. Direct heat source-heat sink simulations

The direct heat source-heat sink method produces a temperature profile of the computer model. The thermal boundary resistance of the interface results in a discontinuity in temperature at the interface, which is visible in the temperature profiles of all the simulations, as shown in Fig. 6. The ratio between the heat flux and the temperature drop at this discontinuity is used to calculate the thermal boundary resistance. As can be seen from Eq. (1), the calculation includes a term for interfacial area, therefore giving a result that is size-independent. Table 2 displays the thermal boundary resistance for each of the direct method simulations. Numbers in brackets are the percent increase with respect to the coherent interface.

To visualize the results, in Fig. 7, we plot the thermal boundary resistance (TBR) of the semi-coherent interfaces as a function of interface area for models with two different specimen sizes. The TBR values of coherent interfaces are also included in the figure for the purpose of comparison. As can be seen from Table 2 and Fig. 7, misfit dislocations have a significant effect on the thermal boundary resistance. Specifically, in the (111) case, the 38-unit cell by 38-unit cell semi-coherent model exhibits a thermal boundary resistance that is 47 % higher than the coherent model; this difference increased with the model size up to 62 % for the 114-unit cell by 114-unit cell model. By contrast, for the (100) lattice direction, the effect is less pronounced, with only about a 10 % difference, increasing to 31 % for the largest model. It is noticed that the thermal resistance for different interface areas has not converged yet, implying that the TBR values may continue to increase for larger interface areas.

Simulation results from the pinned dislocation simulations are summarized in Table 3. The pinned dislocation models exhibit a significantly lower thermal boundary resistance compared to the unpinned ones, a difference of approximately 14 % for each model. The maximum difference of 14.8 % is observed in the (111) 114 by 114 model. The larger model for both lattice directions exhibits a slightly greater reduction in TBR compared to the smaller models. This demonstrates the significant role of dislocation mobility in thermal resistance, implying the dynamic interaction between phonons and dislocations and the effect of their collective behavior on phonon thermal transport.

3.2. Phonon wave propagation simulations

To obtain insights into the simulation results of TBRs using the direct heat-source heat-sink method, we have simulated the propagations of phonon wave packets across the interfaces. Fig. 8 plots the energy transmission coefficients for the TA and LA phonon simulations for both the misfit and the coherent computer models. As can be seen from Fig. 8, the energy transmission of the phonon wave packets across the (111) interface is generally higher than that across the (100) interface. The

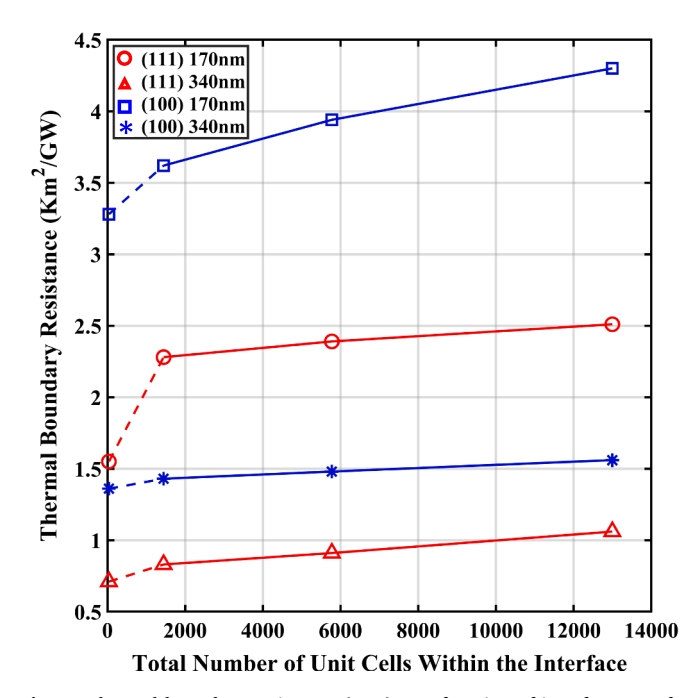


Fig. 7. Thermal boundary resistance (TBR) as a function of interface area for computer models with different lengths. The TBR values for the small coherent interfaces are included for the purpose of comparison. Dashed lines connect the points for the coherent and semi-coherent interfaces.

 Table 3

 Thermal Boundary Resistance for the Pinned Dislocations.

Model		Thermal Boundary Resistance (Km ² /GW)		
Crystal Orientation	Interface Size (unit cells)	Model with Unpinned Dislocations	Model with Pinned Dislocation	
(100)	38 by 38	1.43	1.23	
	114 by 114	1.56	1.35	
(111)	38 by 38	0.83	0.71	
	114 by 114	1.06	0.90	

result is consistent with the simulation results of TBRs, using the direct heat-source heat sink method, i.e., the TBRs of the $(1\,0\,0)$ interfaces are higher than the $(1\,1\,1)$ interfaces. The misfit dislocations in both the $(1\,1\,1)$ and $(1\,0\,0)$ interfaces strongly resonate with the TA phonons, manifested as the local minima of energy transmission. The consistency in the results between the direct heat-source-heat-sink simulations and the wave packet simulations indicates the validity of the results. Also, the much higher energy transmission coefficients for the $(1\,1\,1)$ interface for larger wavevectors, i.e., the higher energy phonons, as shown in Fig. 8 C and D, explains the lower TBRs of the $(1\,1\,1)$ interfaces, and

Table 2
Thermal boundary resistance for interfaces of various areas and two different specimen lengths. The numbers in brackets are the increase in TBR with respect to the corresponding coherent interface.

Model		Thermal Boundary Resistance (Km^2/GW)				
Crystal Orientation	Specimen Length (nm)	6 by 6 unit cells (Coherent)	38 by 38 unit cells	76 by 76 unit cells	114 by 114 unit cells	
(111)	170	1.55	2.28	2.39	2.51	
			(+47 %)	(+54 %)	(+62 %)	
	340	0.71	0.83	0.91	1.06	
			(+17 %)	(+28 %)	(+49 %)	
(100) 170 340	170	3.28	3.62	3.94	4.30	
			(+10 %)	(+20 %)	(+31 %)	
	340	1.36	1.43	1.48	1.56	
			(+5%)	(+9%)	(+15 %)	

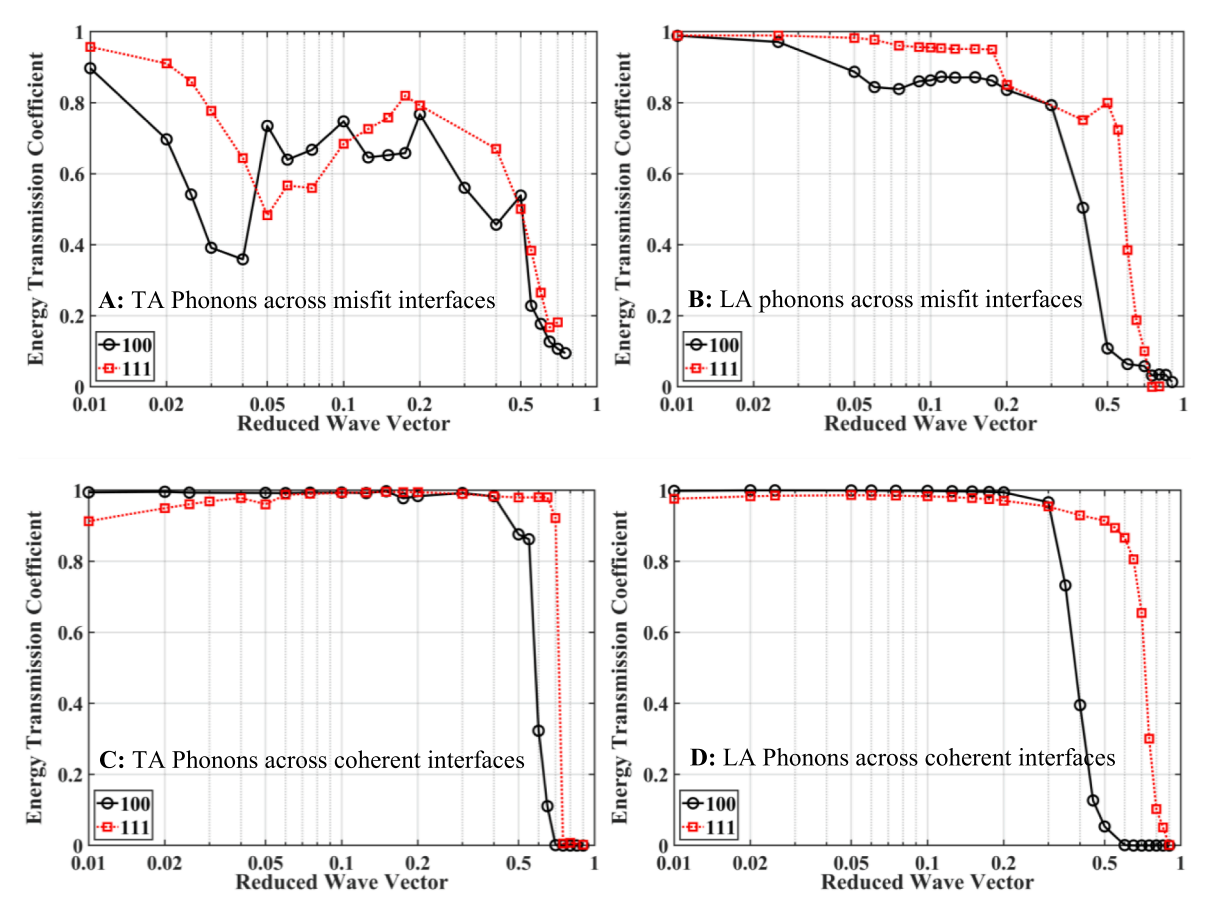


Fig. 8. Plots of the energy transmission coefficients for TA (A) and LA (B) phonon wave packet simulations in the model with the interfacial misfit dislocations, as well as the TA (C) and LA (D) phonon wave packet simulations for the model with the coherent interface.

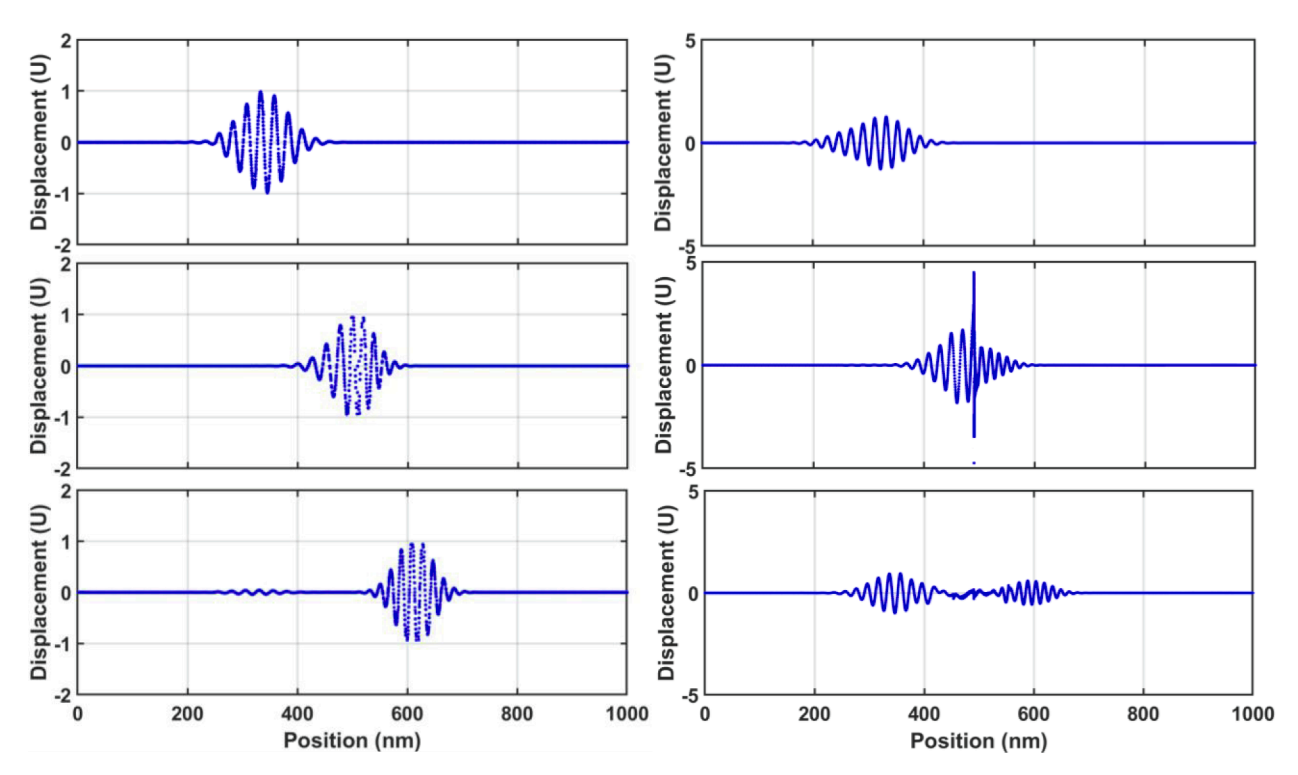


Fig. 9. Time sequences of the displacement field of both the coherent (left) and misfit (right) interfaces for the PbTe/PbSe (100) heterostructure during the propagation of a TA phonon wave packet with a reduced wave vector 0.03. The unit of displacement, U, denotes the amplitude of the phonon wave packet in units of 10^{-3} Å. The interface is located at 500 nm.

subsequently the much greater role of the misfit dislocations in the TBRs of the $(1\,1\,1)$, $62\,\%$ for the $(1\,1\,1)$ interfaces compared with the $31\,\%$ for the $(1\,0\,0)$ interfaces.

To visualize the interaction between phonons and the misfit dislocations, in Fig. 9, we compare the displacement time sequence of a phonon wave packet across the coherent interface with that across the semi-coherent (100) interfaces. The wave packet is centered at a reduced wave vector of 0.03, i.e. close to the minimum in the transmission coefficient in Fig. 8. It has an energy transmission coefficient of 0.982 and 0.392 for the coherent and semi-coherent interfaces, respectively. As can be seen from Fig. 9, the majority of the wave packet transmits across the coherent interface, whereas > 60 % of the wave packet reflects back by the misfit interfaces. Moreover, a large displacement, \sim 5U, where U is the amplitude of the incident wave packet, is observed at the interface when the wave packet meets with the interface, indicating a resonance interaction between phonons and the dislocation networks at the interfaces.

4. Summary and discussions

In this study, we have investigated the thermal boundary resistance of the PbTe/PbSe heterostructures in the (111) and (100) lattice directions. Large-scale MD simulations have been conducted for a variety of specimen dimensions to gain a quantitative understanding of the thermal transport properties of the interfaces. The defect structure and density are obtained through simulations of the direct wafer bonding processes, in good agreement with experimental observations. Major findings on the thermal boundary resistance (TBR) are summarized as follows:

- (1) Misfit dislocations at the PbTe/PbSe interfaces have a significant effect on the room temperature TBR of the interfaces. In particular, there is a 62 % increase in TBR for the PbTe/PbSe (111) system, while a 31 % increase for the PbTe/PbSe (100) system, for the computer model with an interface area of 51.6 nm by 44.7 nm, (i.e., with the 114-unit cells by 114-unit cells).
- (2) The TBR values of the (111) systems are consistently lower than those of the (100) interfaces but are more strongly influenced by the misfit dislocations. This is because the PbTe/PbSe systems are less chemically discontinuous at the (111) interface than that at the (100) interface, as shown in Fig. 1, leading to a much lower TBR at the (111) coherent interfaces, as demonstrated in Table 2. Consequently, we observe a large increase in the contribution of misfit dislocations to TBR at the (111) misfit interfaces with respect to the coherent interface.
- (3) For both systems, the TBR is found to increase with interface area, increasing $\sim 10\,\%$ for the computer model with an interface area of 114-unit cells by 114-unit cells from that with 38-unit cells by 38-unit cells. A possible reason is that a large interface contains a larger dislocation network and hence more vibrational modes of the dislocations. This implies a significant role of the vibrations of the dislocation networks in thermal conductance.
- (4) The room temperature TBR is also found to decrease with the length of the specimen. Doubling the specimen length results in a TBR value of approximately half of the original. Recall that the maximum wavelength of any phonon in a specimen is limited to the specimen's length. Consequently, a longer specimen enables phonons of longer wavelength to reach and traverse the interface. This also indicates that long-wavelength phonons contribute significantly to thermal conductance, a phenomenon of non-Fourier heat conduction at the nano- and micro-scales, as a diffusive heat conduction would be independent of the system's size. Additionally, these results suggest that room temperature TBR for PbTe/PbSe interfaces is not just a property of an interface, but that of the entire structure and the size of the specimen.

(5) The pinned dislocations, which partially reduce the mobility of the misfit dislocations, are shown to reduce thermal resistance, causing ~ 10–15 % lower TBR, as a result of a reduction of dynamic interaction between phonons and dislocations. This demonstrates the collective motion of the dislocation and its significant contribution to the scattering of phonons in the heterostructure.

We would like to note that the simulation results have shown that the thermal boundary resistance has not yet converged for the size of the computer models, including both the area of the interface and the length of the computer model. To obtain a more comprehensive understanding of the effect of interface size on TBR, it would be beneficial to conduct simulations on models with larger interface sizes. However, the 114-unit cell by 114-unit cell model, with over 60 million atoms, is already approaching the computational feasibility limits for MD simulations with the computer resources available to us. Expanding this study would necessitate employing more advanced computational methods, such as Concurrent Atomistic Continuum (CAC) simulations [18,19]. Also, the computer models contain only misfit dislocations at the interfaces, which is true for directly bonded heterostructures. In epitaxially grown heterostructures, there are often both misfit and threading dislocations. The thermal boundary resistance is thus likely much higher in such epitaxial heterostructures than those presented in this study. Additionally, these extra dislocations would also impact the effect of size on thermal boundary resistance.

CRediT authorship contribution statement

Nicholas Taormina: Conceptualization, Data curation, Formal analysis, Investigation, Methodology, Validation, Visualization, Writing - original draft. Yang Li: Conceptualization, Formal analysis, Methodology. Simon Phillpot: Funding acquisition, Methodology, Project administration, Resources, Supervision, Writing - review & editing. Youping Chen: Funding acquisition, Methodology, Project administration, Resources, Supervision, Writing - review & editing.

Declaration of competing interest

The authors declare that they have no known competing financial interests or personal relationships that could have appeared to influence the work reported in this paper.

Data availability

Data will be made available on request.

Acknowledgements

This work is based on research supported by the US National Science Foundation under Award Number CMMI-2054607 through a REU (Research Experiences for Undergraduates) Supplement. The work of YC and SP are also partially supported by DMR 2121895. The computer simulations are funded by the Advanced Cyberinfrastructure Coordination Ecosystem: Services & Support (ACCESS) allocation TG-DMR190008.

References

- [1] J.R. Sootsman, D.Y. Chung, M.G. Kanatzidis, Angew. Chem. Int. Ed. 48 (2009) 8616–8639, https://doi.org/10.1002/anie.200900598.
- [2] H.J. Goldsmid, Introduction to Thermoelectricity, Springer, 2010.
- [3] O. Delaire, J. Ma, K. Marty, A.F. May, M.A. McGuire, M.-H. Du, D.J. Singh, A. Podlesnyak, G. Ehlers, M. Lumsden, Nat. Mater. 10 (2011) 614–619, https://doi. org/10.1038/nmat3035.
- [4] S. Lee, K. Esfarjani, T. Luo, J. Zhou, Z. Tian, G. Chen, Nat. Commun. 5 (2014) 3525, https://doi.org/10.1038/ncomms4525.

- [5] G. Springholz, K. Wiesauer, Phys. Rev. Lett. 88 (2001) 015507, https://doi.org/ 10.1103/PhysRevB.85.184303.
- [6] M.T. Dove (Ed.), Structure and Dynamics: an Atomic View of Materials, Oxford University PressOxford, 2003.
- [7] E. Nadgornyi, Prog. Mater Sci. 31 (1988) 1–530, https://doi.org/10.1016/0079-6425(88)90005-9.
- [8] B.C. Daly, H.J. Maris, K. Imamura, S. Tamura, Phys. Rev. B 66 (2002) 024301, https://doi.org/10.1103/PhysRevB.66.024301.
- [9] J. Garg, G. Chen, Phys. Rev. B 87 (2013) 140302, https://doi.org/10.1103/ PhysRevB.87.140302.
- [10] E. Landry, A. McGaughey, Phys. Rev. B 79 (2009) 075316, https://doi.org/ 10.1103/PhysRevB.79.075316.
- [11] S.C. Huberman, J.M. Larkin, A.J. McGaughey, C.H. Amon, Phys. Rev. B 88 (2013) 155311, https://doi.org/10.1103/PhysRevB.88.155311.
- [12] K. Termentzidis, P. Chantrenne, J.-Y. Duquesne, A. Saci, J. Phys. Condens. Matter 22 (2010) 475001, https://doi.org/10.1088/0953-8984/22/47/475001.
- [13] S.-M. Lee, D.G. Cahill, R. Venkatasubramanian, Appl. Phys. Lett. 70 (1997) 2957–2959, https://doi.org/10.1063/1.118755.
- [14] Y.K. Koh, Y. Cao, D.G. Cahill, D. Jena, Adv. Funct. Mater. 19 (2009) 610–615, https://doi.org/10.1002/adfm.200800984.
- [15] J. Sun, Y. Li, Y. Karaaslan, C. Sevik, Y. Chen, J. Appl. Phys. 130 (2021), https://doi. org/10.1063/5.0049662.
- [16] Y. Li, Z. Fan, W. Li, D.L. McDowell, Y. Chen, J. Mater. Res. 34 (2019) 2306–2314.
- [17] Y. Li, B. Gu, A. Diaz, S.R. Phillpot, D.L. McDowell, Y. Chen, Acta Mater. 260 (2023) 119308, https://doi.org/10.1016/j.actamat.2023.119308.
- [18] Y. Chen, S. Shabanov, D.L. McDowell, J. Appl. Phys. 126 (2019), https://doi.org/ 10.1063/1.5099653.
- [19] A. Diaz, B. Gu, Y. Li, S.J. Plimpton, D.L. McDowell, Y. Chen, J. Comput. Phys. 463 (2022) 111140, https://doi.org/10.1016/j.jcp.2022.111140.

- [20] Y. Chen, J. Chem. Phys. 130 (2009), https://doi.org/10.1063/1.3103887.
- [21] Y. Li, Z. Zheng, A. Diaz, S.R. Phillpot, D.L. McDowell, Y. Chen, Acta Mater. 237 (2022) 118143, https://doi.org/10.1016/j.actamat.2022.118143.
- [22] Z. Fan, R.S. Koster, S. Wang, C. Fang, A.O. Yalcin, F.D. Tichelaar, H. W. Zandbergen, M.A. Van Huis, T.J. Vlugt, J. Chem. Phys. 141 (2014), https://doi.org/10.1063/1.4904545.
- [23] K. Wiesauer, G. Springholz, Appl. Surf. Sci. 188 (2002) 49–54, https://doi.org/ 10.1016/S0169-4332(01)00733-4.
- [24] K. Wiesauer, G. Springholz, Appl. Phys. Lett. 83 (2003) 5160–5162, https://doi. org/10.1063/1.1633675.
- [25] A. Stukowski, Modell. Simulat. Mater. Sci. Eng. 18 (2009) 015012, https://doi.org/ 10.1088/0965-0393/18/1/015012.
- [26] A. Stukowski, K. Albe, Model. Simul. Mater. Sci. Eng. 18 (2010) 085001, https://doi.org/10.1088/0965-0393/18/8/085001.
- [27] A. Anderson, M. Malinowski, Phys. Rev. B 5 (1972) 3199, https://doi.org/ 10.1103/PhysRevB.5.3199.
- [28] E.P. Roth, A.C. Anderson, Phys. Rev. B 20 (1979) 768, https://doi.org/10.1103/ PhysRevB.20.768.
- [29] P.K. Schelling, S.R. Phillpot, P. Keblinski, Phys. Rev. B 65 (2002), https://doi.org/ 10.1103/PhysRevB.65.144306.
- [30] Z. Liang, M. Hu, J. Appl. Phys. 123 (2018), https://doi.org/10.1063/1.5027519.
- [31] X. Chen, A. Diaz, L. Xiong, D.L. McDowell, Y. Chen, J. Comput. Phys. 354 (2018) 393–402, https://doi.org/10.1016/j.jcp.2017.10.038.
- [32] X. Chen, W. Li, L. Xiong, Y. Li, S. Yang, Z. Zheng, D.L. McDowell, Y. Chen, Acta Mater. 136 (2017) 355–365, https://doi.org/10.1016/j.actamat.2017.06.054.
- [33] P. Schelling, S. Phillpot, P. Keblinski, Appl. Phys. Lett. 80 (2002) 2484–2486, https://doi.org/10.1063/1.1465106.